Impact of Charging Conditions and Membrane Thickness on Hydrogen Permeation Through Steel: Thick / Thin Membrane Concepts Revisited

Jean Kittel, Xavier Feaugas, Juan Creus

Impact of Charging Conditions and Membrane Thickness on Hydrogen Permeation Through Steel: Thick / Thin Membrane Concepts Revisited.

Jean Kittel, IFP Energies Nouvelles, Rond-point de l'échangeur de Solaize,
69360 Solaize, BP 3, France

Xavier Feaugas & Juan Creus, LaSIE, UMR CNRS 7356, Université de La Rochelle,
Bat. Marie Curie, Av. Michel Crepeau, 17042 La Rochelle, France

ABSTRACT

This paper develops the relationships between proton reduction at the surface of metals, and hydrogen evolution or hydrogen diffusion into the metal. Equations relating the permeation rate to the proton reduction rate are developed in the case of adsorption – absorption mechanism, with Volmer – Tafel reactions. Analytical expressions are derived, and three distinct regimes are evidenced: i/ a thin membrane – low current domain, where all reduced protons enter into the metal and diffuses to the exit face (i.e. the permeation rate is equal to the faradaic reaction rate) ; ii/ a thin membrane and high current domain, where the permeation rate is proportional to the square root of the proton reduction rate, but is independent of the membrane thickness and, iii/ a thick membrane high current situation, where the permeation rate is still proportional to the square root of the proton reduction rate, and also inversely proportional to the membrane thickness. These permeation regimes and their analytical expressions are then used to examine results published in the literature for α-iron and low alloy steel in different charging environments. It can be shown that the transition between thick and thin membrane regimes and low – high charging conditions are strongly inter-related. It was also possible to establish that governing equations could be described with two main parameters, i.e. a critical membrane thickness and a critical current density. The former appears to depend mainly on the metal properties, while the latter is a direct measure of the ability of the charging media to promote hydrogen entry in the metal.

INTRODUCTION

Since its first development in the sixties, hydrogen permeation has been widely used for the study of interactions between hydrogen and steel or alloys. In aqueous environments, hydrogen is generated by proton reduction either at free corrosion potential or under cathodic polarization. The permeation technique can be used to study metallurgical aspects of hydrogen - steel interactions, in order to develop new steel grades with enhanced resistance to hydrogen embrittlement (HE). Another domain of interest is the study of interactions between corrosive solution and steel, in order to rank the severity of the environment. Analysis of permeation transients is usually done using Fick's laws of diffusion, eventually including additional aspects accounting for hydrogen–defect interactions. In order to avoid misinterpretation of experimental data, it is therefore necessary to have a good knowledge of the leading parameters and of rate determining steps. For example, in order to study bulk metal–hydrogen interactions, it is preferable that the permeation flux measured at the exit face should be under bulk diffusion control. This condition may be achieved by using a steel membrane with a sufficiently high thickness. On the contrary, if the focus is given to studying surface reactions at the entry face, it is better to minimize the kinetic contribution of bulk diffusion, and thus to use thin membranes. Correct knowledge of these aspects is of tremendous importance, since they govern the

boundary conditions for diffusion analysis. Computational analysis has been recently performed by Legrand et al. to evaluate the impact of diffusion limitation induced by oxide formation in the exit size of the membrane and questions the possible interaction between material heterogeneity (grain-boundaries) and thickness of the membrane.[1–3] In both cases the electrochemical kinetics associated with surface activity haven't been considered.
The concepts of thin and thick permeation membranes were introduced by Wach[4] in 1966 and revisited in the early 2000's by Crolet,[5,6] based on permeation experiments on carbon steels exposed to H_2S solutions. For "thick membranes", hydrogen subsurface concentration C_0 is constant, while the permeation flux J_{perm} is inversely proportional to the membrane thickness l. By contrast, for "thin membranes", the permeation regime is governed by the kinetics of hydrogen entry: C_0 becomes proportional to the membrane thickness, while J_{perm} is constant. In mildly acidic aqueous solutions containing dissolved H_2S, the transition between these two permeation regimes was observed experimentally, and it takes place at thicknesses of a few millimeters.[7–9]

In the present work, we propose a more general kinetic formalism to describe the impact of faradaic reactions rate (v_F) associated with electrochemical processes which occur at the entry side and the permeation rate (v_{perm}) obtained at the exit surface. Analytical expressions are derived from the kinetic formulation of hydrogen evolution reaction (HER) and hydrogen absorption reaction (HAR), with the specific aim to define a relationship between v_F and v_{perm}. This approach highlights different permeation regimes, strongly linked with membrane thickness and faradaic reaction rates. Different hydrogen adsorption–absorption models proposed in the literature will be reexamined through this particular link between v_F and v_{perm}. It will be shown that the degree of simplification of the system may lead to false interpretations. In the second part of the paper, experimental data from the literature obtained on α-iron or low alloy steel in different environments will be examined. It will be shown that the model is able to capture a wide range of situations, like situations where the permeation flux is independent of the membrane thickness (d), or on the contrary situations where it is inversely proportional to d. The impact of charging current density and charging media, including the presence of hydrogen entry promoters, will also be illustrated and discussed.

THE FOUNDATIONS: HER – HAR GOVERNING EQUATIONS

Stationary permeation behavior is examined through proton reduction and hydrogen entry theories.[10–14] The analytical framework is focused on the indirect adsorption–absorption mechanism illustrated on Figure 1.

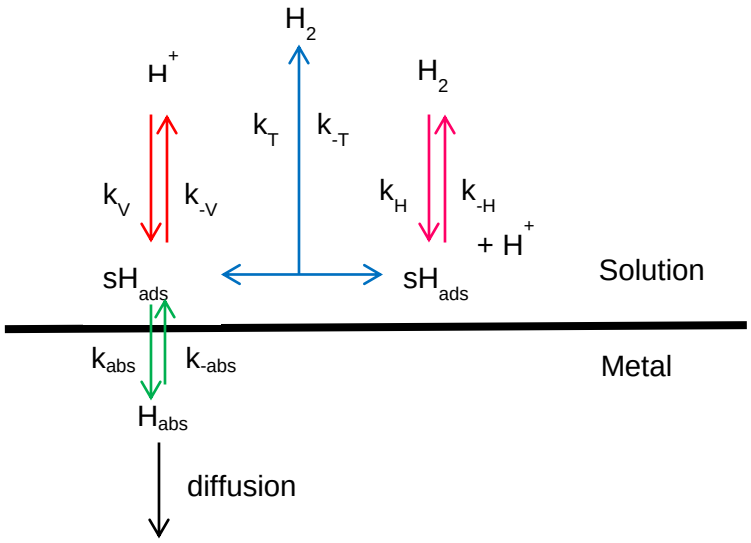

Figure 1: Classical model illustrating proton reduction at a metal surface, followed by hydrogen evolution or hydrogen absorption.

In acid media, it is usually considered that the first step consists in the electrochemical reduction of proton, and results in the formation of an adsorbed intermediate (Volmer reaction):

$$H^+ + s + e^- \underset{k_{-V}}{\overset{k_V}{\rightleftarrows}} sH_{ads} \tag{1}$$

In this reaction, s represents a favorable reaction site at the metal surface. Considering a Langmuir adsorption isotherm, the reaction rate for this reaction is then given by:

$$v_V = k_V(1-\theta) - k_{-V}\theta \tag{2}$$

Where θ is the surface coverage of the metal surface by sH_{ads}. The forward rate coefficient (k_V) depends on proton activity at the metal surface (a_{H+}), temperature (T), and potential (E, referred to the reversible standard hydrogen electrode), while the backward rate coefficient (k_{-V}) only depends on E and T:

$$k_V = a_{H+}\mathrm{k}_V^0 e^{\frac{-\Delta G_{ads}}{RT}} e^{\frac{-\beta_V FE}{RT}} \tag{3}$$

$$k_{-V} = \mathrm{k}_V^0 e^{\frac{\Delta G_{ads}}{RT}} e^{\frac{(1-\beta_V)FE}{RT}} \tag{4}$$

k_V^0, is the intrinsic rate constant for the reaction, ΔG_{ads} is the half-standard free energy of adsorption in aqueous solution, which may depend on the surface coverage θ, β_V is the rate barrier symmetry factor, and F and R are respectively the Faraday constant (F = 96485 C.mol^{-1}) and the ideal gas constant (R = 8.314 J.mol^{-1}.K^{-1}).

Several reactions may then imply the adsorbed intermediate, either leading to gaseous di-hydrogen evolution in the solution, or to hydrogen entry into the metal. Hydrogen evolution may proceed by electrochemical (Heyrowski) or chemical (Tafel) reactions, respectively:

$$sH_{ads} + H^+ + e^- \underset{k_{-H}}{\overset{k_H}{\rightleftarrows}} s + H_2 \tag{5}$$

$$sH_{ads} + sH_{ads} \underset{k_{-T}}{\overset{k_T}{\rightleftarrows}} 2s + H_2 \tag{6}$$

The corresponding reaction rates are then given by:

$$v_H = k_H\theta - k_{-H}(1-\theta) \tag{7}$$

$$v_T = k_T\theta^2 - k_{-T}(1-\theta)^2 \tag{8}$$

In these equations, k_H and k_{-H} admit similar expressions as k_V and k_{-V}, with respective constants k_H^0, β_H. For the chemical combination route, the rate coefficients do not depend on potential, and the fugacity of hydrogen dissolved in the solution (f_{H2}) is introduced:

$$k_T = k_T^0 e^{\frac{2\,\Delta G_{ads}}{RT}} \tag{9}$$

$$k_{-T} = f_{H2} k_T^0 e^{\frac{-2\,\Delta G_{ads}}{RT}} \tag{10}$$

In addition, adsorbed intermediate may also release hydrogen into the metal, by the so-called hydrogen absorption reaction (HAR):

$$sH_{ads} \underset{k_{-abs}}{\overset{k_{abs}}{\rightleftarrows}} s + H_{abs} \tag{11}$$

The reaction rate of this reaction depends on the surface coverage, but also on the degree of saturation of the metal just below the surface, C_0/C_{max}, where C_0 is the concentration of H_{abs} at a depth $x = 0$ below the surface and C_{max} is the maximum concentration which can be hosted into the metal. Then, the absorption reaction rate is expressed as the difference between a charging flux and a desorption flux:

$$v_{abs} = k_{abs}\theta\left(1 - \frac{C_0}{C_{max}}\right) - k_{-abs}(1-\theta)\left(\frac{C_0}{C_{max}}\right) \tag{12}$$

With:

$$k_{abs} = k_{abs}^0 e^{\frac{(\Delta G_{ads} - \Delta G_{diss})}{RT}} \tag{13}$$

$$k_{-abs} = k_{abs}^0 e^{\frac{(\Delta G_{ads} - \Delta G_{diss})}{RT}} \tag{14}$$

Within this theoretical framework, hydrogen evolution (HER) and absorption (HAR) are fully described by reactions (1), (5), (6) and (11), and the steady-state behavior can be determined through their respective reaction rates (2), (7), (8) and (12). In this system, the rate of the faradaic reactions (v_F) is obtained as the sum of v_V and v_H.

THEORETICAL DEVELOPMENT

System studied: linear diffusion through planar metal membrane

The steady-state study proposed hereafter is applied to a planar metal membrane of thickness d. One face of this membrane is exposed to an electrolyte where HER and HAR are likely to occur. A perfect hydrogen extraction method is applied on the other face. It is also considered that hydrogen diffusion in the metal proceeds perpendicular to the surface, and trapping is not taken into account.
At steady state, hydrogen concentration at the entry face is C_0, and its value at the exit face is equal to zero. The hydrogen permeation rate at the exit side is then given by:

$$v_{perm} = D\frac{C_0}{d} \tag{15}$$

Where D is the diffusion coefficient of hydrogen in the metal.
Steady-state also implies that hydrogen fluxes at the entry and exit sides are equal:

$$v_{abs} = v_{perm}. \tag{16}$$

Combining equations (12) (15) and (16) leads to a simple relationship between the hydrogen concentration and the surface coverage:

$$\frac{C_0}{(C_{max}-C_0)} = \frac{k_{abs}\theta}{\frac{DC_{max}}{d}+k_{-abs}(1-\theta)} \tag{17}$$

Which may be more easily manipulated in its opposite form, after introduction of v_{perm} with equation (15):

$$\frac{1}{v_{perm}} = \frac{d}{DC_{max}}\left[1+\frac{k_{-abs}}{k_{abs}}\left(\frac{1-\theta}{\theta}\right)\right]+\frac{1}{k_{abs}\theta} \tag{18}$$

Steady-state also applies to reactions at the entry face, and corresponds to:

$$v_V = v_{perm} + 2v_T + v_H \tag{19}$$

Equations (17) and (19) represent the common starting point of many papers dealing with hydrogen entry mechanisms with HER – HAR theories. [15–17] This whole system is however quite complex, and difficult to solve analytically unless simplifying hypotheses are considered. Since many different roads can be taken to simplify the system, a broad range of theories were raised, sometimes leading to conflicting results. For example, the early work of Bockris *et al.* considered a low surface coverage ($\theta \ll 1$), dilute absorbed hydrogen in the metal subsurface ($C_0 \ll C_{max}$), and control by diffusion of hydrogen through steel membrane (which corresponds to $DC_{max}/e \ll k_{-abs}$). They also made the additional hypothesis that hydrogen evolution proceeded only via the Tafel reaction, and that the absorption flux was negligible compared to the hydrogen evolution flux ($v_{perm} \ll v_F$). Later, other authors proposed similar analysis with less restrictive hypothesis, and presented their results as “new models”. In fact, most of these models are affiliated to the same initial equations (18) and (19), and they only differ by the degree and type of simplifying hypothesis.
It is therefore the goal of this paper to re-examine step by step this hydrogen adsorption - absorption model, beginning with the most simple. A specific focus will be placed on establishing

the relationship between the hydrogen diffusion flux through a metal membrane and the rate of proton reduction, and studying the impact of membrane thickness. The analysis performed in this paper still contains simplifications on the hydrogen evolution reactions. For carbon steel it is generally admitted that the main route is Volmer – Tafel at low overpotential (low surface coverage), and that it moves to Tafel – Heyrowski at high cathodic overpotential (high surface coverage). [15,16] Only the first route is examined in this paper, thus corresponding to $k_H = k_{-H} = 0$. It is further assumed that the Volmer and Tafel backward reactions are negligible ($k_{-V} = k_{-T} = 0$). With these assumptions, equation (19) may be simplified to:

$$2k_t\theta^2 - k_V(1-\theta) + v_{perm} = 0 \tag{20}$$

Or, introducing the faradaic reaction rate (v_F) which in this specific case is equal to the Volmer reaction rate, one obtains a useful relationship relating the surface coverage to v_F and v_{perm}, which are easily measurable parameters :

$$\theta = \frac{\sqrt{v_F - v_{perm}}}{\sqrt{2k_t}} \tag{21}$$

This expression reflects the surface coverage arising from the Volmer– Tafel hydrogen entry route without backward reactions, which is the reference situation considered in this paper. Equations (20) or (21) are therefore used in the various case studies considered hereunder.

Case study #1: Bockris model

Our analysis starts by meeting with the pioneer model of Bockris *et al.* [16] which corresponds to the highest degree of simplification of equation (17). The assumptions made by these authors were the following: i/ low surface coverage ($\theta \ll 1$), ii/ dilute absorbed hydrogen in the metal subsurface ($C_0 \ll C_{max}$), iii/ hydrogen diffusion is the rate determining step ($DC_{max}/d \ll k_{-abs}$), and iv/ permeation current is low compared to the faradaic current ($v_{perm} \ll v_F$).
With these assumptions, equations (17) and (21) become respectively:

$$\frac{C_0}{C_{max}} = \frac{k_{abs}}{k_{-abs}}\theta \tag{22}$$

$$\theta = \frac{\sqrt{v_F}}{\sqrt{2k_t}} \tag{23}$$

Combining these equations and introducing v_{perm} with equation (15) results in the well-known Bockris expression where the absorption (permeation) rate and the square root of the hydrogen evolution reaction are proportional:

$$v_{perm} = \frac{k_{abs}}{k_{-abs}} \times \frac{DC_{max}}{d} \times \frac{\sqrt{v_F}}{\sqrt{2k_t}} \tag{24}$$

In that case, the permeation rate is also inversely proportional to the membrane thickness, which is a direct consequence of diffusion control.
The simplicity of the resulting equations, combined with the renown of its authors and the pioneer character of the work have resulted in an intensive and sometimes abusive use of this model. Indeed, the simplifying hypotheses and the resulting severe limitations of the validity

domains of equation (18) must not be forgotten to avoid erroneous interpretations. According to hypotheses i/ to iv/ the validity domain of Equation (24) is defined by:

$$\sqrt{v_F} \ll \sqrt{2k_t} \tag{25}$$

$$\sqrt{v_F} \ll \sqrt{2k_t}\, k_{-abs}/k_{abs} \tag{26}$$

$$d \gg d_{crit} = DC_{max}/k_{-abs} \tag{27}$$

$$v_F \gg \left(\frac{k_{abs}}{k_{-abs}} \times \frac{DC_{max}}{d}\right)^2 \times \frac{1}{2k_t} = \left(k_{abs} \times \frac{d_{crit}}{d}\right)^2 \times \frac{1}{2k_t} \tag{27}$$

This model presents strong limitations related to the faradaic current, which presents an upper (Equations [25] or [26]) and a lower (Equation [28]) limit. It also requires that the metal membrane be thicker than a critical value (d_{crit}) defined by Equation (27). This critical thickness depends on hydrogen solubility (C_{max}) and diffusivity (D) in the metal, as well as on the absorption backward reaction rate (k_{-abs}). Since it depends mainly on bulk properties of the metal, this critical thickness should not vary with the environmental conditions and can be considered an intrinsic property of a given metal.

Case #2: extension of Bockris model to low current

As illustrated in the previous case, the hypothesis that the permeation current is negligible compared to the cathodic current strongly reduces the validity domain of the model. A quite simple and direct extension of the Bockris model can therefore be proposed where v_{perm} is not neglected in equation (21). All other hypotheses are similar to the previous case. Expression of v_{perm} is thus obtained by combining (15), (21) and (22):

$$\frac{2k_t}{{k_{abs}}^2}\left(\frac{d}{d_{crit}}\right)^2 {v_{perm}}^2 + v_{perm} - v_F = 0 \tag{29}$$

Introducing $K_1(d) = \frac{2k_t}{{k_{abs}}^2}\left(\frac{d}{d_{crit}}\right)^2$, the positive solution of this polynomial expression of v_{perm} is given by:

$$v_{perm} = \frac{\sqrt{1+4K_1(d)v_F}-1}{2K_1(d)} \tag{30}$$

The validity domain for this expression is still related to hypothesis i/ to iii/ of previous case, with limits defined by equations (25) through (27). At high faradaic current, similar results as case #1 are found, i.e. proportionality of v_{perm} with the square root of v_F. Nevertheless, excluding hypothesis iv/ from the initial simplification allows extending the validity domain to low current. Analysis of expression (30) then shows that if the faradaic current is sufficiently low, the permeation rate becomes equal to the faradaic rate:

$$v_{perm} = v_F \tag{31}$$

Interestingly, the impact of membrane thickness on the permeation rate vanishes, indicating a change of rate determining step from diffusion through the bulk to surface reactions. The

transition between the low current region where $v_{perm} = v_F$ and the high current region where $v_{perm} \propto {v_F}^{1/2}$ is easily determined as:

$$v_{Ftrans} = \left(\frac{d_{crit}}{d}\right)^2 \times \frac{{k_{abs}}^2}{2k_t} \tag{32}$$

This transition is highly influenced by the membrane thickness, as v_{Ftrans} is inversely proportional to d^2.

Case 3: Extension to thin membranes

The first two cases considered only situations where metal membranes had a high thickness ($d \gg d_{crit}$), in order to simplify the denominator of Equation (17). Nevertheless, since the value of d_{crit} is usually not known, most of permeation studies are performed without *a priori* knowledge of the validity of assumption iii/. It seems therefore important to establish the global equations, regardless the membrane thicknesses. This situation is similar to the model developed by Iyer, Pickering and Zamanzadeh, also referred to as IPZ model.[17] Keeping hypothesis of low surface coverage ($\theta \ll 1$) and dilute absorbed hydrogen ($C_0 \ll C_{max}$), equation (18) becomes:

$$\frac{C_{max}}{C_0} = \frac{k_{-abs}}{k_{abs}\theta} + \frac{DC_{max}}{dk_{abs}\theta} \tag{33}$$

Replacing C_0 and θ with v_{perm} and v_F (using equations [15] and [21]) and introducing d_{crit} (equation [27]) finally results in:

$$\frac{2k_t}{{k_{abs}}^2}\left(1 + \frac{d}{d_{crit}}\right)^2 {v_{perm}}^2 + v_{perm} - v_F = 0 \tag{34}$$

whose solution is:

$$v_{perm} = \frac{\sqrt{1+4K_2(d)v_F}-1}{2K_2(d)} \tag{35}$$

where $K_2(d)$ corresponds to:

$$K_2(d) = \frac{2k_t}{{k_{abs}}^2}\left(1 + \frac{d}{d_{crit}}\right)^2 \tag{36}$$

Similarly to case 2, the low current limit of v_{perm} is v_F, while it takes the form $v_{perm} \propto \sqrt{v_F}$ at high current. The transition between both regions is close to the previous one (equation [32]), except that it includes a constant limit for thin membranes (i.e. for $d \ll d_{crit}$):

$$v_{Ftrans} = \left(1 + \frac{d}{d_{crit}}\right)^{-2} \times \frac{{k_{abs}}^2}{2k_t} \tag{37}$$

It should be noticed that when $d \ll d_{crit}$, the impact of membrane thickness on v_{perm} disappears both in the low faradaic current region (where $v_{perm} = v_F$) and in the high current domain, where equation (35) simplifies to $v_{perm} = \mathrm{k}_{abs}\sqrt{v_F/2k_t}$. In a similar manner as d_{crit} earlier, a critical

faradaic current corresponding to the limit of equation (37) for thin membranes can be defined as:

$$v_{Fcrit} = \frac{{k_{abs}}^2}{2k_t} \tag{38}$$

The final expression (35) relating the permeation current density to the faradaic current density can finally be rewritten with v_{Fcrit} and d_{crit} as only independent parameters as:

$$v_{perm} = \frac{\sqrt{1+4\frac{v_F}{v_{Fcrit}}\left(1+\frac{d}{d_{crit}}\right)^2}-1}{\frac{2}{v_{Fcrit}}\left(1+\frac{d}{d_{crit}}\right)^2} \tag{39}$$

It follows that a transition membrane thickness (d_{trans}) may also be proposed. Analysis of the limits of equation (33) at low or high membrane thickness results in:

$$\frac{d_{trans}}{d_{crit}} = \sqrt{\frac{v_F}{v_{Fcrit}}} \times \frac{2}{\sqrt{1+4v_F/v_{Fcrit}}-1} \tag{40}$$

For $d \ll d_{trans}$, the permeation flux is independent of the membrane thickness, and is given by:

$$v_{perm} = v_{Fcrit}\frac{\sqrt{1+4v_F/v_{Fcrit}}-1}{2} \tag{41}$$

As expected, the low current limit of this expression corresponds to $v_{perm} = v_F$.
On the other hand, when $d \gg d_{trans}$, an expression for v_{perm} similar to that determined in Case 1 is obtained (equation [24]). Introducing the new notions of critical current and critical thickness gives:

$$v_{perm} = \frac{d_{crit}}{d}\sqrt{v_F v_{Fcrit}} \tag{42}$$

Summary

Main characteristics of the different permeation regimes

The preceding analysis allowed determining the analytical expression relating hydrogen permeation to the net hydrogen reduction faradaic current and to the membrane thickness, for a coupled Volmer–Tafel reaction and at low surface coverage and dilute absorbed hydrogen. Equation (39) fully describes the evolution of the permeation rate was a function of the faradaic reaction rate and the membrane thickness, with d_{crit} and v_{Fcrit} as independent parameters. These cases are illustrated respectively on Figure 2 and Figure 3.

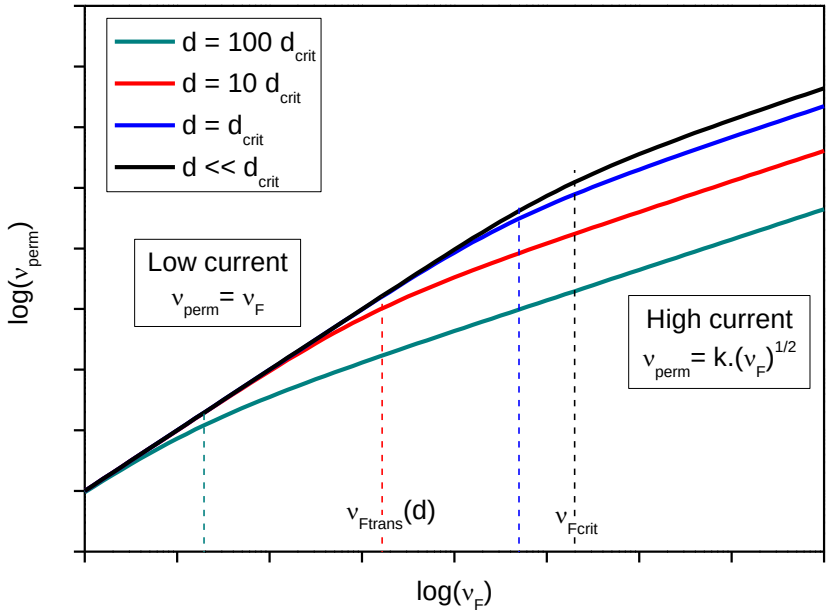

Figure 2: theoretical evolution of v_{perm} with v_F for different values of membrane thickness, corresponding to case 3 above (low surface coverage and low dilute absorbed hydrogen in the metal subsurface).

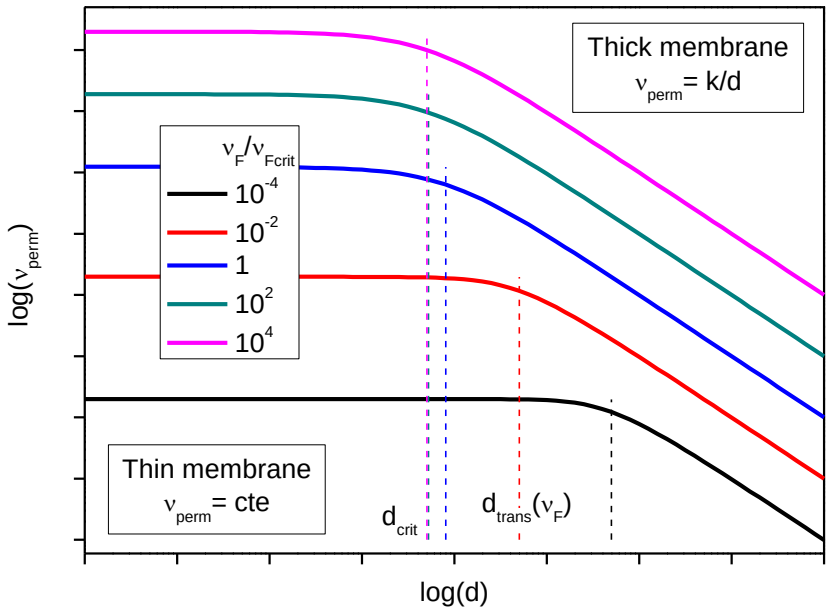

Figure 3: theoretical evolution of v_{perm} with d for different values of v_F, corresponding to case 3 above (low surface coverage and low dilute absorbed hydrogen in the metal subsurface).

It appears that two kinds of characteristic permeation regimes can be defined. Taking the membrane thickness as an independent parameter, thin or thick behaviors correspond respectively to a permeation rate which does not depend on the membrane thickness or to a regime where it is inversely proportional to the membrane thickness. Similarly, considering the charging current density, the low current behavior in characterized by a linear dependence between v_{perm} and v_F, while the high current region corresponds to v_{perm} being proportional to

$\sqrt{v_F}$. Figure 4 illustrates the transitions between these different regions in the $log(v_F) - log(d)$ plane. Since the frontiers between the thin–thick domain and between the low–high current domain share a common part, it is possible to define three sub-domains, respectively thin membrane + low current, thin membrane + high current, and high current + thick membrane. The detailed expressions relating the permeation current density to membrane thickness and charging current density are summarized in Table 1.

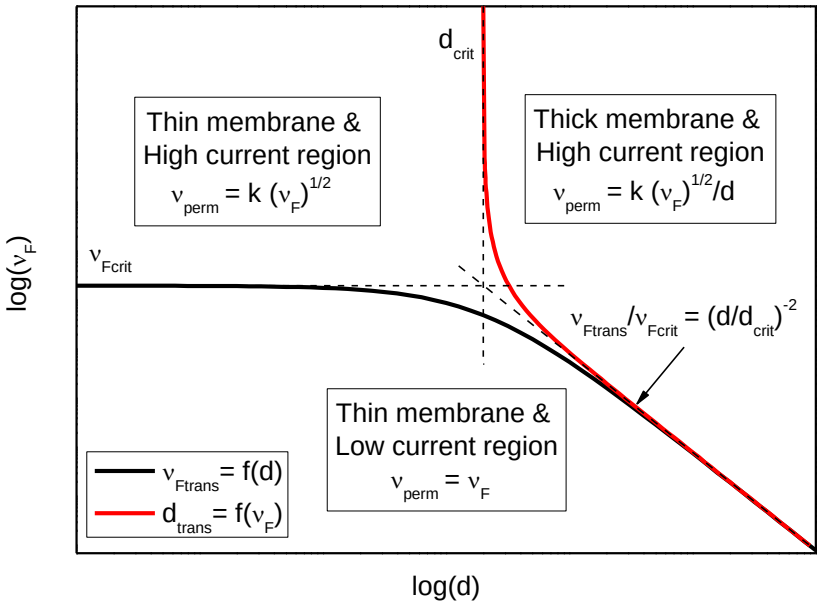

Figure 4: Illustration of the different permeation domain depending on the membrane thickness and on the faradaic current density.

Table 1
Summary of the evolution of permeation regime with membrane thickness and faradaic current density.

	Thin membrane	Thick membrane	Transition thickness
High current	$v_{perm} = \sqrt{v_F v_{Fcrit}}$	$v_{perm} = \left(\frac{d_{crit}}{d}\right)\sqrt{v_F v_{Fcrit}}$	$d_{trans} = d_{crit} = \frac{DC_{max}}{k_{-abs}}$
Low current	$v_{perm} = v_F$		$d_{trans} = d_{crit}\sqrt{\frac{v_{Fcrit}}{v_F}}$
Transition current	$v_{Ftrans} = v_{Fcrit} = \frac{{k_{abs}}^2}{2k_t}$	$v_{Ftrans} = v_{Fcrit}\left(\frac{d_{crit}}{d}\right)^2$	

Apart from the charging current density and the membrane thickness, the only other influencing parameters are the critical thickness and the critical faradaic current. Interestingly, the former depends only on the metal properties ($d_{crit} = DC_{max}/k_{-abs}$), and the latter relates only to surface reaction ($v_{Fcrit} = {k_{abs}}^2/2k_t$). It is therefore quite easy to examine the impact of material properties (through D and C_{max}) or the impact of surface reactions (i.e. action of hydrogen entry promoters or poisons to the recombination).

ANALYSIS OF LITERATURE DATA ON STEEL MEMBRANES

Equation (39), which defines the links between permeation rate and faradaic reaction rates, will now be used to analyze results from the literature. All rate constants used in previous expressions could easily be transformed into current densities after a simple multiplication by the Faraday constant. In the next section of the paper, we will therefore use current densities (J_x) instead of rate constants (v_x) for all reactions (denoted by index x). This analysis is focused on iron and steel but could easily be extended to other types of metals. In all cases, experiments were performed with a palladium deposed at the exit side of permeation membranes, so that it can be considered that the extraction reaction is never rate limiting, which is an important hypothesis of the model developed in the first part of the paper. It must be remarked also that most experimental data which were used for the analysis were obtained with annealed α-iron, which contains a low density of traps (essentially dislocations). Indeed, hydrogen–metal interactions could introduce strong bias when compared to our model which considers only pure diffusion.

Cathodic charging on iron or steel membranes in H_2SO_4 solution

An interesting study was presented by Dillard in 1970, using the Devanathan and Stachurski method to study hydrogen diffusion in pure iron. [18] His experiments were performed in 1N H_2SO_4 as charging solution, which also contained a strong hydrogen entry promoter (5 mg/L As_2O_3). Various experiments were performed, using membrane thickness or cathodic current density as variables. Although not formally identified at that time, these results already illustrated the thin / thick membrane or low / high current transitions. For example, the results of Figure 5 present the evolution of the permeation rate (P expressed in $cm^3.cm^{-2}.s^{-1}$, which can be converted into µA/cm² by dividing P by 1.16 x 10^{-7}) with the square root of the charging current density, for membrane thicknesses varying between 0.25 and 2 mm. In echo to the Bockris postulate, the author interpreted the linear trend above 2 mA/cm² as a proof that the mechanism contained an intermediate adsorption step. However, even if these data were obviously smoothed, a deviation to the linear dependence is noticed at low current, and attributed by the author to an artifact associated with reduction of arsenic to hydride. However, this behavior may also account for a low current region, where v_{perm} becomes equal to v_F. Similarly, this set of results also shows a thin / thick membrane transition. In order to illustrate this transition, we have plotted on Figure 6 the evolution of the permeation rate with the membrane thickness, for a cathodic current density of 9 mA/cm², taken from the results of Figure 5. A transition is clearly visible between thin membrane (constant current) and thick membrane (permeation current inversely proportional to d) regions. A good fit with the model developed in the first part of this paper was obtained, with a critical current density (J_{Fcrit}) of 2 mA/cm² and a critical thickness of 0.45 mm.

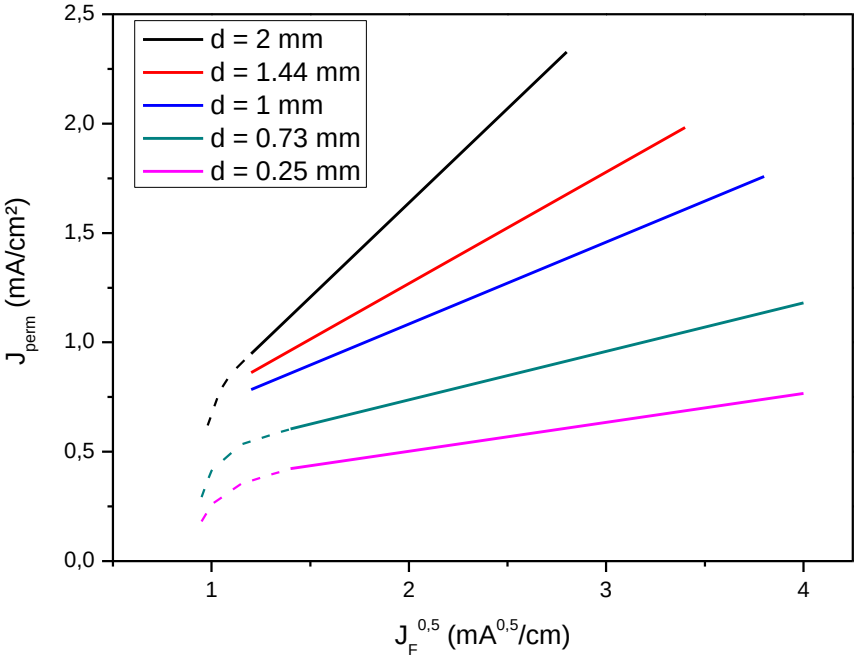

Figure 5: Evolution of the stationary permeation rate with the square root of the cathodic charging current density (1N H_2SO_4 + 5 mg/L As_2O_3), for pure iron membranes of different thickness (data from Dillard [18]).

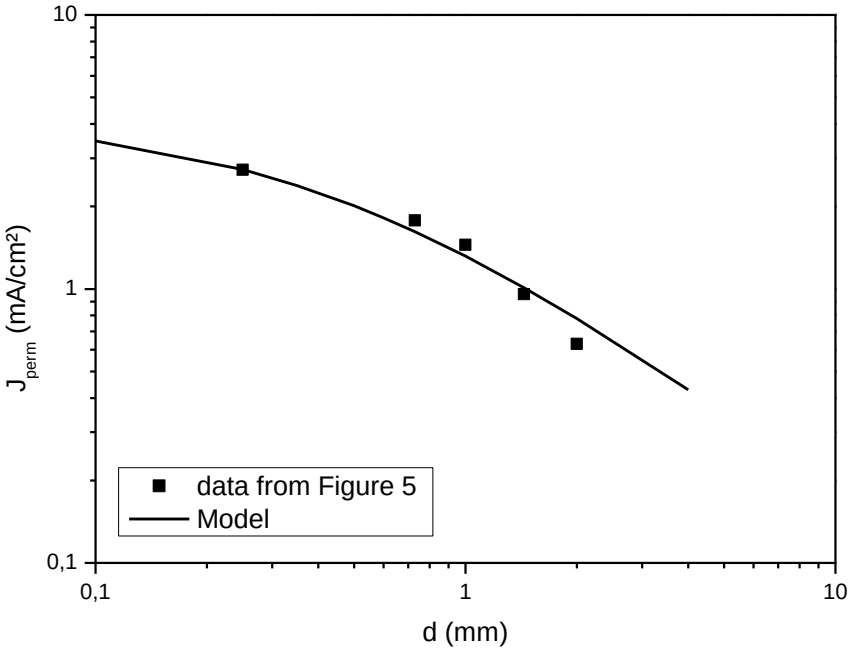

Figure 6: Evolution of the permeation current density with the membrane thickness, from the results of Figure 5 at 3 $mA^{1/2}.cm^{-1}$ (i.e. a cathodic current of 9 mA/cm²). Comparison with the model, with d_{crit}= 0.45 mm and v_{Fcrit}= 2 mA/cm².

Another study with Armco iron membranes of different thicknesses (0.2 to 2 mm) under cathodic charging in 1N H_2SO_4 solution was presented by Antaño-Lopez *et al.* [19] A linear relationship between $J_{perm}$and $1/d$ was observed in all experimental domain, i.e. for cathodic current density between 1 and 10 mA/cm² and membrane thickness between 2 and 0.2 mm (Figure 7). This

behavior is representative of a thick membrane regime. According to the model developed in this paper, and after transformation of reaction rates into current densities, the slope of J_{perm} vs. $1/d$ is equal to: $d_{crit}\sqrt{J_F J_{Fcrit}}$ (see Table 1). Assuming that the critical thickness form the Armco iron membrane is in the same order of that determined for pure iron from the work of Dillard (d_{crit}= 0.45 mm), analysis of the results of Figure 7 gives a critical current density of a few µA/cm² for this charging medium.

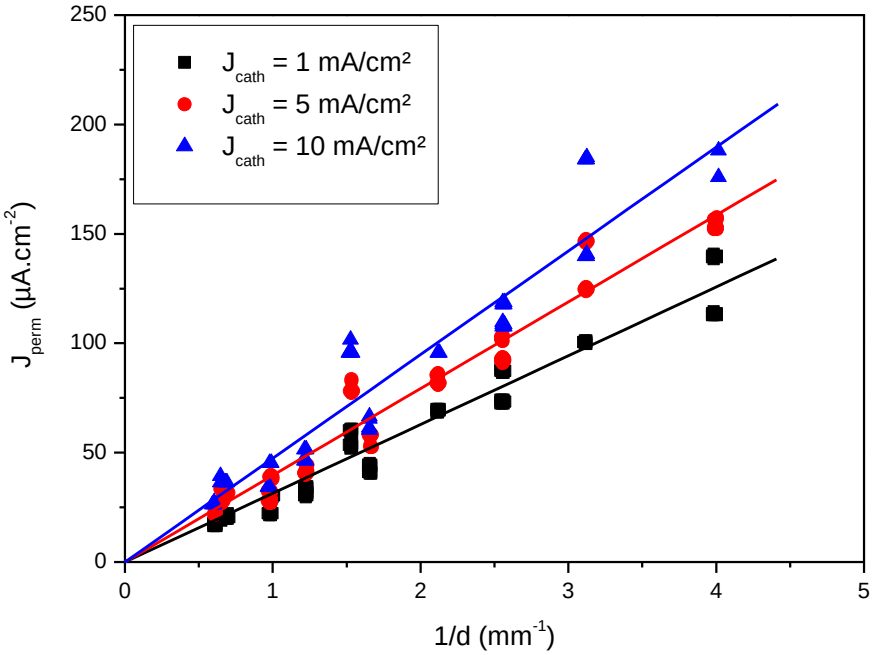

Figure 7: Steady state permeation fluxes through Armco iron membranes of various thickness for respectively -1 (a), -5 (b) and -10 mA/cm² (c) cathodic charging in 1 N H_2SO_4, fromAntaño-Lopez [19].

In comparison, permeation experiments presented by Bockris were realized in 0.1 N H_2SO_4 with 0.77 mm Armco iron membranes, and for charging current densities between 0.5 and 10 mA/cm². As expected, these experimental conditions are definitely inside the high current / thick membrane domain for this metal / environment system. Similar behavior is also found in two other papers by Radahakrishnan and Shreir and by Jérome where the membrane thickness was taken as variable and with a constant charging current density in 0.1 N H2SO_4.[20,21]

Hydrogen permeation in H_2S environments

Oil and gas environments containing CO_2 and H_2S represent a very important industrial domain for hydrogen embrittlement. H_2S is indeed a well-known promoter of hydrogen entry into steels, which can proceed even at the free corrosion potential. In these environments, it has often been observed that the permeation rate did not follow the Bockris predictions (i.e. $J_{perm} \propto \sqrt{P_{H_2}}$ or $\sqrt{J_F}$). Situations where the permeation rate was independent of the membrane thickness have been reported frequently, and were attributed to a change of rate determining step from surface reactions to bulk hydrogen diffusion[4] The thick–thin membrane concept was then reintroduced in the early 2000's, and experimental data showing a transition thickness of a few millimeters were produced.[5,6,8,9] It seems however possible to analyze more deeply some of the past results, using the concepts of critical and transition thickness and charging current density.

In 2004, Duval *et al.* presented a study combining corrosion rate and permeation measurements for 0.5 mm Armco iron membranes exposed to mildly acidic solutions (pH 2.7 to 6.5) with dissolved H_2S.[8] All experimental data were plotted in a graph representing the evolution of the steady-state permeation current density with the corrosion current density (J_{corr}), which can be considered equal to proton discharge rate in this media. At low current, a linear trend between J_{perm} and J_{corr} was observed (Figure 8). In addition, these authors performed permeation measurements in similar conditions with membrane thickness up to 1.5 mm, and observed that permeation fluxes did not vary. It can therefore be considered that the results of Figure 8 correspond to a thin membrane situation, and equation (41) may be applied. Applying this correlation allows to determine a critical current density in the order of 200 µA/cm². Since it is believed that this value is mainly related to surface reactions, it should be applicable to other experimental data obtained on steel in acid solutions with dissolved H_2S, at least in the range 0.1 – 1 bar.

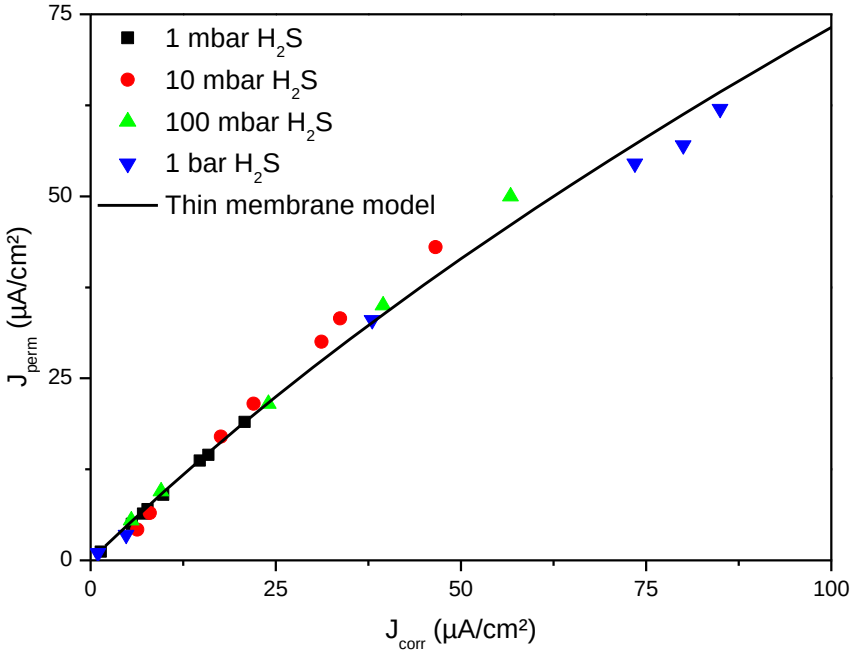

Figure 8: Permeation current vs. corrosion current density for a 0.5 mm thick steel membrane exposed to acid water with dissolved H_2S (from Duval [8]). Comparison with the predictions of equation (41) (thin membrane model) with J_{Fcrit} = 200 µA/cm².

Another series of experimental data obtained in the same lab and in similar conditions was presented by Kittel et al.[9] In this paper, low alloy steel membrane thickness was varied from 0.5 to 10 mm, and a transition between a constant flux (i.e. independent of the membrane thickness) and a flux inversely proportional to the membrane thickness was evidenced. Experimental permeation current densities obtained on two different steel grades exposed to pH 3.5 and pH 5.5 test solution (100 mbar H_2S) are plotted on Figure 9. Analysis of these results was performed with equation (39), with the same value of J_{Fcrit} as that determined from the preceding analysis of the results of Antaño-Lopez (J_{Fcrit} = 200 µA/cm²). Only d_{crit} was used as adjustable parameter in order to obtain the best fit between calculated and experimental data. The best results were obtained with d_{crit} = 1 mm for steel A (sour grade), and d_{crit} = 0.7 mm for steel B (sweet grade), which are rather similar as the value for Armco iron. Using these values for d_{crit} and J_{Fcrit}, one easily determines the transition thickness for these experimental conditions, using equation (40). The results show that d_{trans} varies between 1.2 and 2.6 mm,

which is in very good agreement with the transition observed experimentally. It must be remarked that since the charging current densities for these experiments were not sufficiently high to be in the “high current domain”, this transition thickness does not correspond to the critical thickness.

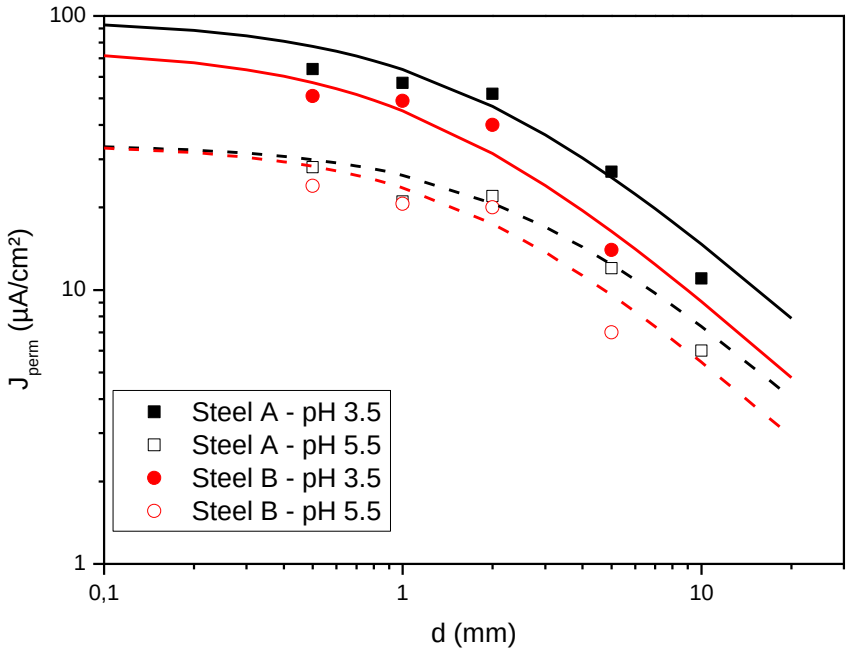

Figure 9: Illustration of the impact of membrane on the steady state permeation flux for different experiments under 100 mbar H_2S and 900 mbar CO_2 (from Kittel [9]), and comparison with calculated permeation rates (equation [39]).

The last sets of data from the literature used for our analysis combine H_2S environment in mildly acidic solutions and cathodic charging. Some of these results date 1963, by Le Boucher, and were obtained on extremely thin mild steel membranes exposed to 10 mM NaCl solutions containing 6.7 to 7.1 mM H_2S (i.e. close to the solubility of 50 mbar H_2S in gas phase), at pH between 4.35 and 4.55.[22,23] The second experimental study was presented by Plennevaux *et al.*, and was realized on 0.5 mm high strength steel membranes, exposed to 0.1M $NaClO_4$ solution at pH 4.5 (acidified by $HClO_4$) with different levels of H_2S, between zero and 50 mbar.[24,25] The results obtained by these authors during cathodic polarization are presented on Figure 10 and Figure 11.

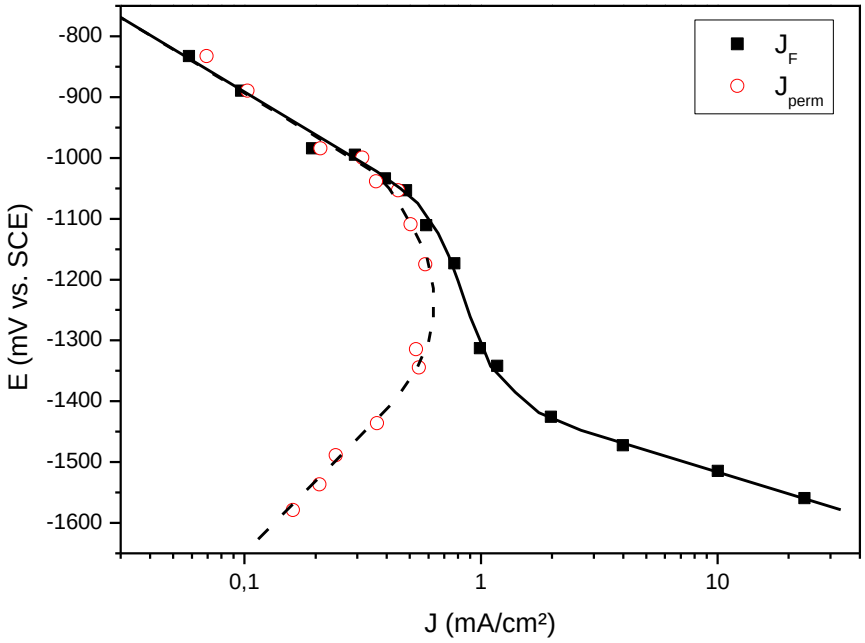

Figure 10: Comparison between the evolution of the cathodic current density and the permeation current density with the electrode potential, measured on 0.04 mm mild steel membranes exposed to 10 mM NaCl solution with 6.5 mM dissolved H_2S and at pH 4.35 (data from Le Boucher[22]).

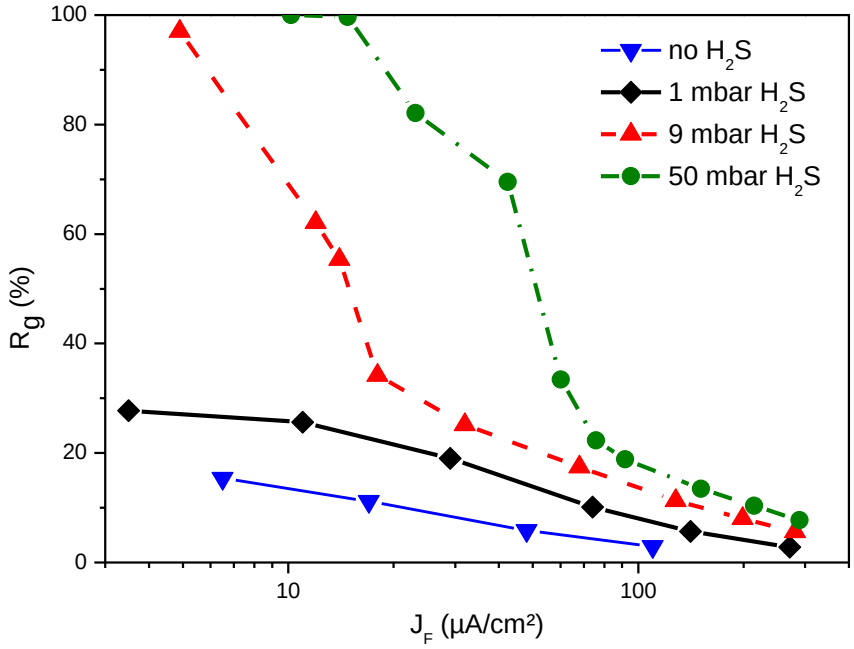

Figure 11 :Evolution of the permeation efficiency ($R_g = J_{perm}/J_F$) with the cathodic current density, measured on 0.5 mm high strength steel membrane exposed to pH 4.5 solutions with varying H_2S levels, from Plennevaux.[25]

Analysis of polarization curves presented by Le Boucher (Figure 10) shows that the permeation rate is equal to the cathodic current density at low overpotential, i.e. a thin membrane – low current behavior. A deviation is observed when the current density is close to 0.3-0.6 mA/cm². Since the membrane thickness for this study is well below the critical thickness determined

previously for similar types of steels, it can be considered that this transition current density corresponds to the critical current density in this environment (i.e pH 4.5 and close to 50 mbar H_2S). In similar conditions with 50 mbar H_2S but with a membrane ten times thicker, Plennevaux et al. observed that the transition happened in the cathodic current domain between 20 and 80 µA/cm² (Figure 11). This transition is in good agreement with the predictions of the model (equation [37]), using d_{crit} = 0.5 mm and J_{Ftrans} = 0.3 to 0.6 mA/cm².
Furthermore, the results of Figure 11 also illustrate the impact of decreasing the concentration of H_2S. Under 9 mbar H_2S, the transition is observed at lower cathodic current density, i.e. between 5 to 20 mA/cm², and it further decreases at lower H_2S. This effect can only be due to a decrease of the critical current density, i.e. to a decrease of the promotion of hydrogen charging by H_2S.

Summary and discussion

Even though the model developed in this paper is probably oversimplified, it has been used successfully to analyze literature data on iron and low alloy steel membranes in different charging media at acid pH. The orders of magnitude of critical thickness for iron and low alloy steel have been evaluated, as well as critical current densities for different charging solutions (Table 2). From different independent studies in various charging conditions, the critical thicknesses were relatively identical for pure iron, Armco iron, or low alloy steels, with values between 0.5 and 1 mm. This confirms that this parameter is essentially related to the metal properties. On the other hand, critical current densities were found to vary by several orders of magnitude by changing the charging solution composition. The lowest v_{Fcrit} was observed in pure H_2SO_4 solutions, with values of a few µA/cm². Since this cathodic current level is well below the corrosion current density of mild steels in concentrated H_2SO_4, it explains why a thin membrane or low current behavior has never been observed experimentally for a steel / H_2SO_4 system, whatever the membrane thickness. Addition of a well-known hydrogen entry promoter (As_2O_3) to the H_2SO_4 solution was found to affect dramatically J_{Fcrit}, with an increase of three orders of magnitude (J_{Fcrit} =2 mA/cm² from the work of Dillard [18]). The same effect was found in mildly acid (pH 4.5) solutions containing H_2S with a decrease of J_{Fcrit} with P_{H2S}, from several hundreds of µA/cm² at 50 mbar H_2S, down to less than a few µA/cm² at 1 mbar H_2S and below. J_{Fcrit} can thus be considered as the main parameter representative of the ability of the charging solution to promote hydrogen entry in the metal.
It can be noted also that this analysis opens news paths between the “adsorption - absorption” and the direct entry model for hydrogen entry. Indeed, it can be noticed that the low current situation of the adsorption – absorption model presents strong similarities with the “direct entry model” attributed to Bagotskaya and Frumkin [26–29] or the “direct entry through adsorbate” first introduced by Le Boucher to explain the action of HS^- ions on hydrogen embrittlement, and then extended to other promoters.[22,23,30] Both models predict a linear relationship between v_{perm} and v_F and independence with membrane thickness at low cathodic current. Thus, the arguments brought forward by Bockris to justify the invalidity of the direct entry model do not stand.[16] On the other hand, it also appears that both theories may give rise to similar expressions for v_{perm}, and it is therefore not possible to make a call between these two views at this stage. On the other hand, whatever the true mechanism of hydrogen entry promoters, their action can be modelled by an increase of the critical current density, which could either result from an increase of k_{abs} (direct entry theory), or to a decrease of k_t (poison to recombination, or adsorption site blocking theory).

Table 2
Summary of literature data: experimental conditions and results of d_{crit} and J_{Fcrit} evaluations with this model.

Ref.	Material / thickness	Charging conditions	d_{crit}/ v_{Fcrit}
[18]	Pure iron / 0.25 – 2 mm	1 N H_2SO_4 + 5 mg/L As_2O_3 J_F = 1 – 10 mA/cm²	d_{crit} = 0.45 mm J_{Fcrit}= 2 mA/cm²
[19]	Armco iron / 0.2 – 2 mm	1N H_2SO_4 J_F = 1 – 10 mA/cm²	J_{Fcrit}= 1-4 µA/cm² [a]
[16]	Armco iron / 0.77 mm	0.1N H_2SO_4 J_F = 0.5 – 10 mA/cm²	No transition observed
[8]	Armco iron / 0.5 – 1.5 mm	0.5% acetic acid + 5% NaCl pH range 2.7 – 6 P_{H2S} 1 mbar to 1 bar	J_{Fcrit} = 200 µA/cm² [b] (for 100 mbar to 1 bar H_2S)
[9]	Low alloy steel / 0.5 – 10 mm	0.4% sodium acetate + 5% NaCl pH range 3.5 – 5.5 P_{H2S} 3 mbar to 100 mbar	d_{crit} = 0.7 to 1 mm [c]
[22]	Mild steel / 0.04 – 0.2 mm	10 mM NaCl + 50 mbar H_2S pH 4.5	J_{Fcrit} = 0.3 – 0.6 mA/cm² [b]
[25]	Low alloy steel / 0.5 mm	$HClO_4$ + 0.1 M $NaClO_4$ pH 4.5 P_{H2S} 0 – 50 mbar	d_{crit} = 0.5 mm [d] J_{Fcrit} decreases when P_{H2S} decreases

[a] for the calculation of this parameter from experimental data, a value of d_{crit} = 0.45 mm was postulated, by analogy with analysis of the results of Dillard.[18]
[b] this parameter was determined independently of d_{crit}, since the experimental conditions were in the thin membrane domain.
[c] for the calculation of this parameter, a value of v_{Fcrit} = 200 µA/cm² was postulated, by analogy with analysis of the results of Duval.[8]
[d] for the calculation of this parameter, a value of v_{Fcrit} = 300 µA/cm² was postulated, by analogy with analysis of the results of Le Boucher.[22]

CONCLUSIONS

The analysis performed in this paper aimed at studying relationships between proton reduction occurring at the surface of metals under cathodic polarization, and the resulting hydrogen diffusion in the metal. The primary objective was to identify limiting situations depending on the thickness of the diffusion media (membrane thickness) and on the intensity of faradaic surface reactions (proton reduction). Analytical expressions were developed in the case of a coupled adsorption – absorption route with the Volmer–Tafel reactions. Three main permeation regimes were characterized: i/ a thin membrane – low current domain, where all reduced proton enters into the metal and diffuses to the exit face ($v_{perm} = v_F$) ; ii/ a thin membrane and high current domain, where the permeation rate is proportional to the square root of the proton reduction rate, but, independent of the membrane thickness and, iii/ a thick membrane high current situation, where v_{perm} is still proportional to $\sqrt{v_F}$, and also inversely proportional to the membrane thickness. It was also possible to establish the expressions (valid for the Volmer-Tafel route) defining the transitions between each of these domains, either as a function of membrane

thickness or as a function of faradaic reaction rate. These transitions are strongly inter-related. It was also possible to define a critical thickness d_{crit}, linked with the metal properties, and a critical current density J_{Fcrit}, related to the charging environment, from which all governing equations could easily be expressed. The order of magnitude of d_{crit} was determined between 0.5 and 1 mm, for α-iron and low alloy steels (ferrite – pearlite microstructure) from literature data in various charging environments. Values of critical current densities were also evaluated, and it was confirmed that it was strongly linked with the ability of the environment to promote hydrogen charging. This parameter could therefore represent an excellent candidate to rank the severity of any environment for hydrogen charging and the associated risks of hydrogen embrittlement.

It can finally be noted that even if the analysis presented in this paper was restricted to the adsorption – absorption route with Volmer – Tafel reactions, it could easily be reproduced for other electrochemical pathways, or for other hydrogen entry theories. Nevertheless, the main conclusions are not expected to change dramatically by changing the intermediate reactions, since the different regimes evidenced in this paper only reflect kinetic control by surface reactions or by bulk diffusion.

ACKNOWLEDGEMENTS

Grateful acknowledgement is made to S. Frappart for fruitful discussions before preparation of this manuscript. A special thank is also addressed to C. Plennevaux, whose PhD results have inspired the reflections developed in this paper.

REFERENCES

1. E. Legrand, J. Bouhattate, X. Feaugas, H. Garmestani, International Journal of Hydrogen Energy 37, 13574–13582 (2012).
2 E. Legrand, J. Bouhattate, X. Feaugas, S. Touzain, H. Garmestani, M. Khaleel, D.S. Li, Computational Materials Science 71, 1–9 (2013).
3. E. Legrand, A. Oudriss, S. Frappart, J. Creus, X. Feaugas, J. Bouhattate, International Journal of Hydrogen Energy 39, 1145–1155 (2014).
4. S. Wach, A.P. Miodownik, J. Mackowiak, Corrosion Science 6, 271–285 (1966).
5. J.L. Crolet, M.R. Bonis, Revisiting hydrogen in steel, part II: experimental verifications, Corrosion 2001 paper 01072, 11-16 March, Houston, TX (USA), NACE International (2001).
6. J.L. Crolet, M.R. Bonis, Revisiting hydrogen in steel, part I: theoretical aspects of charging, stress cracking and permeation, Corrosion 2001 paper 01067, 11-16 March, Houston, TX (USA), NACE International (2001).
7. J. Kittel, F. Ropital, J. Pellier, New insights into hydrogen permeation in steels: measurements through thick membranes, Corrosion 2008 paper 08409, 16-20 March, New-Orleans, LO (USA), NACE International (2008).
8. S. Duval, R. Antano-Lopez, C. Scomparin, M. Jerome, F. Ropital, Hydrogen permeation through ARMCO iron membranes in sour media, Corrosion 2004 paper 04740, March 28 - April 1, New-Orleans, LO (USA), NACE International (2004).
9. J. Kittel, F. Ropital, J. Pellier, Corrosion 64, 788–799 (2008).
10. A. Lasia, A. Rami, Journal of Electroanalytical Chemistry and Interfacial Electrochemistry 294, 123–141 (1990).
11. C. Gabrielli, G. Maurin, L. Mirkova, H. Perrot, Journal of Electroanalytical Chemistry 590, 15–25 (2006).

12. C. Gabrielli, G. Maurin, L. Mirkova, H. Perrot, B. Tribollet, Journal of Electroanalytical Chemistry 590, 1–14 (2006).
13. H. El Alami, J. Creus, X. Feaugas, Electrochimica Acta 51, 4716–4727 (2006).
14. B.E. Conway, in: B.E. Conway, R.E. White, J.O. Bockris (Eds.), Modern aspects of electrochemistry, Plenum Press, New York, pp. 103–185 (1985).
15. M.A.V. Devanathan, Z. Stachurski, Journal of the Electrochemical Society 111, 619–623 (1964).
16. J.O. Bockris, J. McBreen, L. Nanis, Journal of the Electrochemical Society 112, 1025–1031 (1965).
17. R.N. Iyer, H.W. Pickering, M. Zamanzadeh, Journal of the Electrochemical Society 136, 2463–2470 (1989).
18. J.L. Dillard, Mémoires Scientifiques de la Revue de Métallurgie 67, 767–775 (1970).
19. R. Antano-Lopez, S. Duval, M. Jerome, J. Galland, F. Ropital, Hydrogen permeation in iron membranes under various charging conditions including wet H_2S, Eurocorr 2003, 28 September - 2 October, Budapest (Hungary), The European Federation of Corrosion (2003).
20. T.P. Radhakrishnan, L.L. Shreir, Electrochimica Acta 12, 889–903 (1967).
21. M. Jérôme, Intéractions hydrogène - métal et perméation électrochimique: Mémoire d'HDR de l'Université de Technologie de Compiègne (2003).
22. B. Le Boucher, Revue de l'Institut Francais du Petrole 23, 1–66 (1963).
23. B. Le Boucher, Catalytic action of HS- chemisorbed ions on iron in corrosion processes, 4th International Congress on Metallic Corrosion, 550–555 (1972).
24. C. Plennevaux, J. Kittel, M. Frégonèse, B. Normand, F. Ropital, F. Grosjean, T. Cassagne, Electrochemistry Communications 26, 17–20 (2013).
25. C. Plennevaux, Etude des risques de corrosion ete de rupture différée des aciers en présence d'H_2S dans les conditions d'exploration de pétrole et de gaz à haute pression et haute température: Thèse de l'INSA de Lyon, France (2012).
26. A.N. Frumkin, in: P. Delahay (Ed.), Advances in electrochemistry and electrochemical engineering, Interscience Publishers, Inc., New-York (USA), p. 393 (1963).
27. I.A. Bagotskaya, Zhur. Fiz. Khim., 2667 (1962).
28. P. Bai, S. Zheng, H. Zhao, Y. Ding, J. Wu, C. Chen, Corrosion Science 87, 397–406 (2014).
29. G. Zheng, B.N. Popov, R.E. White, Journal of the Electrochemical Society 142, 154–156 (1995).
30. T. Zakroczymski, Z. Szklarska-śmiałowska, M. Śmiałowski, Materials and Corrosion 27, 625–630 (1976).